

# A first-principles approach to electrical transport in atomic-scale nanostructures

J. J. Palacios\*, A. J. Pérez-Jiménez\*\*, E. Louis\*, E. SanFabián\*\*, and J. A. Vergés\*\*\*

\**Departamento de Física Aplicada, Universidad de Alicante, San Vicente del Raspeig, Alicante 03690, Spain*

\*\**Departamento de Química-Física, Universidad de Alicante, San Vicente del Raspeig, Alicante 03690, Spain*

\*\*\**Instituto de Ciencia de Materiales de Madrid (CSIC), Cantoblanco, Madrid 28049, Spain.*

(November 10, 2021)

We present a first-principles numerical implementation of Landauer formalism for electrical transport in nanostructures characterized down to the atomic level. The novelty and interest of our method lies essentially on two facts. First of all, it makes use of the versatile Gaussian98 code, which is widely used within the quantum chemistry community. Secondly, it incorporates the semi-infinite electrodes in a very generic and efficient way by means of Bethe lattices. We name this method the Gaussian Embedded Cluster Method (GECM). In order to make contact with other proposed implementations, we illustrate our technique by calculating the conductance in some well-studied systems such as metallic (Al and Au) nanocontacts and C-atom chains connected to metallic (Al and Au) electrodes. In the case of Al nanocontacts the conductance turns out to be quite dependent on the detailed atomic arrangement. On the contrary, the conductance in Au nanocontacts presents quite universal features. In the case of C chains, where the self-consistency guarantees the local charge transfer and the correct alignment of the molecular and electrode levels, we find that the conductance oscillates with the number of atoms in the chain regardless of the type of electrode. However, for short chains and Al electrodes the even-odd periodicity is reversed at equilibrium bond distances.

## I. INTRODUCTION

Molecular- and atomic-scale electronic devices are attracting an ever increasing interest due to the impact they are expected to make in the world of Nanotechnology. The number of experimental and theoretical works in this particular area of research, generically known as molecular electronics [1], is growing exponentially. The design of devices at the molecular and even atomic scale poses new challenges which require new theoretical and experimental techniques to be developed. Scanning Tunneling Microscopy (STM) is probably the pioneer of the experimental techniques in this research area. It can be used not only in the tunneling regime to image adsorbates [2,3], but also in the contact regime to build few-atom nanoscopic contacts [4]. STM can also be used to investigate the electrical properties of nanotubes [5] and DNA molecules [6] with one or both of their ends attached to a suitable electrode. In addition to STM, mechanically controllable break junctions have also revealed themselves as powerful tools to study electrical transport in metallic nanobridges [7] or individual molecules [8,9].

The basics to calculate the zero-bias conductance  $G$  of a nanoscale contact had been established by Landauer's in his pioneering work [10] long before these systems were commonplace. In Landauer's formalism  $G$  is simply given by the quantum mechanical transmission of the electrons around the Fermi energy [11]. The value of this transmission is essentially determined by the region where the number of channels available for conduction is the smallest. In molecular or atomic-scale nanocontacts the region of relevance is the molecule and/or the few atoms forming the nanoscopic bridge between electrodes. The

transmission is thus strongly dependent on the particular molecule, the detailed atomic arrangement of the electrodes in the contact region, and the chemical nature of them. Knowing the atomic arrangement of the electrodes or the way the molecule binds to the electrodes is, however, a major problem in itself. Furthermore, even if these important details were known, implementing Landauer's formalism still requires to know the electronic structure and this is a formidable task as well.

Calculations based on tight-binding or semi-empirical models [12–14] have been, and still are, very popular since these models capture the atomic-scale character in some detail and are easy to implement. However, they do not allow for structural relaxations to be performed. Most importantly, these simple models, in general, do not yield correct values for the local electronic charges. In other words, the chemical potential is not uniform across the entire system in equilibrium. While imposing local charge neutrality is a straightforward improvement on these models for metallic nanoconstrictions [13,14], there does not exist any simple modification in the case of more complex systems like metal-molecule-metal heterostructures [15]. A way around this problem is to perform self-consistent first-principles calculations which, at least at a mean-field level, guarantee the uniformity of the chemical potential. However, most numerical implementations commonly used to carry out *ab-initio* electronic calculations are either restricted to finite systems, such as the Gaussian code [16], or require the infinite system to be periodic such as the SIESTA code [17]. None of these methods are suitable to address the systems here studied which are both infinite and non-periodic. Finally, a perhaps more serious difficulty is the intrinsic

non-equilibrium character of electrical transport.

In recent years several proposals have appeared to tackle this problem [18–23]. Most of all are based upon density functional (DF) theory. In addition to the well-known virtues of the DF theory, it presents the additional advantage that Landauer’s theoretical framework does not need to be modified since DF is still a single-particle description of the many-body problem. In the pioneering works of Lang and co-workers, Tsukada and co-workers, and Guo and co-workers [18,19,24–26] the electrodes were described within the jellium approximation. Jellium models are still used today [21,27,28]; for they are convenient in one way: They provide featureless contacts which represent generic situations. As mentioned below this is one major feature of our model too. However the jellium model presents serious drawbacks. How can the differences observed experimentally between, for instance, Al and Au electrodes, be taken into account by means of a jellium? Furthermore, this approach is not satisfactory when one is trying to describe, for instance, STM experiments where the detailed atomic structure of the tip determines, to a large extent, whether or not the STM can resolve the topography or molecular structure of the adsorbate. Recent approaches, which essentially differ only on the numerical implementation, intend to incorporate the atomic structure of the electrodes in the DF calculation [20,22,23,29,30]. It is pertinent noting here that in most of these studies a periodic structure beyond a given point within the leads is assumed. Efficient transfer matrix techniques [31,32] make this reasonable assumption tractable, but it forces one to consider a very specific type of lead (typically a finite-section wire [20,22,29,30] or an infinite surface [23]). Using a jellium model for the electrodes is harmless but it lacks the minimum atomic detail which is crucial to describe, e.g., the contact with molecules. However, employing well-defined specific electrodes is not desirable either since their own electronic structure can interfere with the interpretation of the results. For instance, the appearance of gaps in the conductance close to the Fermi energy for perfectly conducting systems such as Au chains can only be considered an artifact due to the unphysical electrode model [22,30]. Furthermore, actual nanocontacts are not expected to have high symmetry. As explained below these difficulties are circumvented in our method.

Recently [33], we have presented an alternative to the *ab-initio* methods above mentioned. Close in spirit to those presented in Refs. [20,22], the main differences and advantages with respect to them are the use of the standard Gaussian98 code to carry out the DF calculation of the relevant transport region and the description of the electrodes bulk by means of appropriate Bethe lattices [34,35]. The Gaussian98 code provides a versatile method to perform first-principles calculations of clusters, incorporating the major advancements in the field in terms of functionals, basis sets, pseudopotentials, etc.. On the

other hand, the Bethe lattices are two-fold convenient: (i) They reproduce the essential features of the bulk density of states and (ii) their directional self-energies can be easily calculated (see Appendix). In Ref. [33] these ideas were applied to investigate electrical transport of a C<sub>60</sub> molecule in between Al electrodes. Here we describe in detail an improvement to our previous approach [33] which can be summarized in that we now incorporate self-consistently the semi-infinite electrodes into the conductance calculation within the Gaussian98 code. This requires working with Green’s functions from the very start. The method has some resemblance with the cluster Bethe lattice method developed to investigate the physical properties (electronic structure, phonons, etc.) of disordered systems [35]. We illustrate the possibilities of our method by investigating electronic transport in Al and Au nanocontacts. These systems have been the subject of extensive studies in the past by means of tight-binding methods [13,14] and, more recently, by means of *ab-initio* methods [21,22,30]. We show that, even in these systems where charge transfer is apparently unessential, tight-binding methods may fail to provide a correct quantitative picture. It turns out that the conductance in the case of Al nanocontacts is strongly dependent on the detailed atomic structure. In the case of Au nanocontacts, on the contrary, the results are more universal as confirmed by experiments. Next, we choose a system with somewhat appealing features: Carbon-atom chains. As shown in Ref. [24] these chains, when contacted by Al electrodes, exhibit a conductance that oscillates with the number of atoms in the chain. Here we address this problem by taking proper account of the binding to the electrodes and investigate how the results depend on the type of electrode (Al or Au).

The rest of the paper is organized as follows. In Section II we discuss the main characteristics of our method. Section III is devoted to an extensive discussion of the results. Finally, we end the paper by summarising the main features of the method and the most remarkable results (Section IV).

## II. THE GAUSSIAN EMBEDDED CLUSTER METHOD (GECM)

In previous work [33] we have presented a method to study transport in atomic-scale and molecular devices which is based on standard quantum chemistry calculations with the Gaussian98 code [16]. This scheme, which has been recently adopted by other groups (see, e.g., Refs. [36]), is taken here a step further. A DF calculation of the region that includes the molecule or set of atoms forming the contact between electrodes and a significant part of the electrodes is performed (see Fig. 1). As far as transport is concerned, the hamiltonian (or Fock matrix  $\hat{F}$ ) of this central cluster or supermolecule contains the relevant

information since it embraces the region with the smallest number of channels for conduction. However, according to the usual theoretical transport schemes [10], its associated Green's functions are unsuitable for the evaluation of the current (note that they simply have poles). The retarded(advanced) Green's functions associated with  $\hat{F}$  needs to be extended to include the rest of the semi-infinite electrodes:

$$\hat{G}^{r(a)}(\epsilon) = (\epsilon \hat{I} \hat{S} - \hat{F} \pm i\delta)^{-1} \rightarrow [\epsilon \hat{I} \hat{S} - \hat{F} - \hat{\Sigma}^{r(a)}(\epsilon)]^{-1}. \quad (1)$$

In this expression

$$\hat{\Sigma}^{r(a)}(\epsilon) = \hat{\Sigma}_R^{r(a)}(\epsilon) + \hat{\Sigma}_L^{r(a)}(\epsilon), \quad (2)$$

where  $\hat{\Sigma}_R(\hat{\Sigma}_L)$  denotes a self-energy matrix that accounts for the part of the right(left) semi-infinite electrode which has not been included in the DF calculation.  $\hat{S}$  is the overlap matrix and  $\hat{I}$  is the unity matrix. The added self-energy matrices can only be explicitly calculated in ideal situations, which, in principle, limits the desired applicability of the above procedure. For instance, in Refs. [22,30] the authors consider finite-section wires as electrodes. As a result of this choice gaps appear in the conductance of otherwise perfectly conducting central clusters.

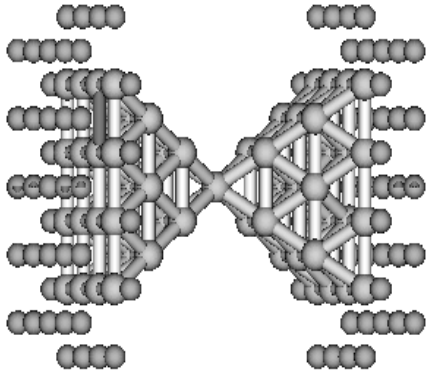


FIG. 1. Schematic view of a cluster where phantom atoms from the Bethe lattices are shown.

In order to overcome this type of problem, we choose to describe the bulk electrode with a Bethe lattice tight-binding model with the appropriate coordination numbers and parameters (see Appendix). The advantage of choosing a Bethe lattice resides in that it reproduces fairly well the bulk density of states of any metallic electrode, avoiding this way the appearance of spurious results. In addition to this the self-energy matrices that appear in Eq. 1 can be calculated iteratively in a simple way (see Appendix for more details). For each atom of the outer planes of the cluster, we choose to add a branch of

the Cayley tree in the direction of any missing bulk atom (including those missing in the same plane). In Fig. 1 the directions in which branches are added are indicated by smaller atoms which represent the first atom of the branch in that direction. Assuming that the most important structural details of the electrode are included in the central cluster, the Bethe lattices should have no other relevance than that of introducing a featureless reservoir.

In our present approach the self-consistent process does not stop once the finite central cluster has been solved. Instead, we reformulate the Gaussian98 code to proceed with the self-consistency of the now infinite system. More specifically, once self-consistency for the finite cluster has been almost attained, we calculate the Green's function as explained above. Then, the density matrix is obtained from the Green's function according to

$$\hat{n} = -\frac{1}{\pi} \int_{-\infty}^{\epsilon_F} \text{Im} [\hat{G}^r(\epsilon)] d\epsilon, \quad (3)$$

where  $\epsilon_F$  is the Fermi level fixed by the condition of overall charge neutrality in the cluster. The integral in Eq. (3) is calculated along a contour in the complex plane as explained in Refs. [20,22,23] with an efficient automatic numerical integration scheme of Pérez-Jordá *et al.* [37]. The density matrix is now used to recalculate the matrix elements of the Fock's operator and the process is repeated until self-consistency is achieved. We note that in this method the standard eigenvalue problem, inherent to the Gaussian98 code, is replaced by the calculation of Green's functions. In the end the Green's functions describe an infinite system in a more consistent way than in the method discussed previously by us [33] since it effectively removes finite-size effects in the self-consistency. It is interesting to note that the applicability of this approach, which we hereafter name the Gaussian Embedded Cluster Method (GECM), goes well beyond the present study. In fact it could be a powerful tool whenever an infinite media has to be described (for instance adsorption of molecules on solid or liquid surfaces).

The conductance can now be simply calculated through the expression [10]

$$G = \frac{2e^2}{h} \text{Tr}[\hat{T}], \quad (4)$$

where Tr denotes the trace over all the orbitals of the cluster and  $\hat{T}$  is the transmission matrix which, in turn, is given by

$$\hat{T} = \hat{\Gamma}_L \hat{G}^r \hat{\Gamma}_R \hat{G}^a, \quad (5)$$

where the matrices  $\hat{\Gamma}_R$  and  $\hat{\Gamma}_L$  are given by  $i(\hat{\Sigma}_R^r - \hat{\Sigma}_R^a)$  and  $i(\hat{\Sigma}_L^r - \hat{\Sigma}_L^a)$ , respectively. In order to single out the contribution of individual channels to the current one can diagonalize the transmission matrix. It turns out

(see below) that only few channels give a non-negligible contribution to the current. The symmetry of each channel was identified by looking at its weight on the atomic orbitals of the central atom of the constriction or the C chain.

Finally, it is worth pointing out that if the current in the finite-bias regime has to be obtained, one should simply integrate in energy the above expression with appropriate Fermi distributions functions. Note, however, that a new definition of the density matrix generalized to non-equilibrium [20,22,23] needs to be used in the calculation of the Green's functions. Apart from this, the Landauer-type expression (4) remains valid as long as one does not give up the single-particle description. In this work we are concerned with basic and still open aspects of transport in the systems studied and we will focus on the linear regime.

### III. RESULTS

For all the DF calculations we have used the Becke's three-parameter hybrid functional using the Lee, Yang and Parr correlation functional (B3LYP) [38] together with the semilocal shape consistent pseudopotential (SCPP) and basis sets of Christiansen *et al.* [39–41]. We have selected this combination of exchange-correlation functional and pseudopotential for two reasons: First, B3LYP is one of the most accurate and certainly the most popular among the gradient-corrected exchange-correlation functionals; second, Christiansen *et al.* SCPP provide accurate results for a wide variety of atoms while retaining the simplicity of a minimal basis set [39–42]. Needless to say that there is no need to restrict the calculations to a minimal basis set since the Bethe lattice can be constructed for any basis set. It is only a matter of computational convenience that we have done it so. Nevertheless, in some cases, we have checked that better basis sets and the use of other exchange-correlation functionals do not modify the main conclusions of our work.

In all cases we have investigated the influence of the number of electrode atoms included in the DF calculation on the conductance. In general, the results do not vary qualitatively with the cluster size, allowing us to extract some general conclusions. However, at a quantitative level, this is not always the case, particularly for Al nanocontacts. Finally we note that, although most of the calculations were carried out taking the bulk interatomic distances for the electrode atoms, in some cases we investigated the effects of *ab-initio* relaxations.

#### A. Metallic nanocontacts

A complete theoretical study of electrical transport in metallic atomic contacts requires a realistic modelization of the formation process of these nanocontacts. Some structural studies using molecular dynamics [43] for Al and *ab-initio* relaxations for Al [44] and Na [45] have been reported. This is, however, a problem beyond the scope of this work. Here we consider archetypical atomic structure models that are likely to appear in the last stages of the formation process of atomic contacts before the break-up: Single-atom contacts and atomic wires. More specifically, our first structure consists of two opposite pyramids grown in the (001) direction and “glued” by a single atom [see Fig. 2]. Single-atom contacts have been studied in the past with modified tight-binding models [13]. We find to our surprise that, even in this simple case, our *ab-initio* results are qualitatively different from those obtained with these models, particularly for Al. Our second structure is similar to the previous one, but with a chain of three atoms instead of a single atom [see Fig. 3]. Finally we have studied the same chain in between two (111) surfaces with the chain placed on top of a surface atom [see Fig. 4]. A similar geometry has been recently studied with *ab-initio* techniques for Au and Al. Our results agree with what has been reported for Al using a jellium model for the electrodes [21], but not entirely with what has been obtained for Au [22,30].

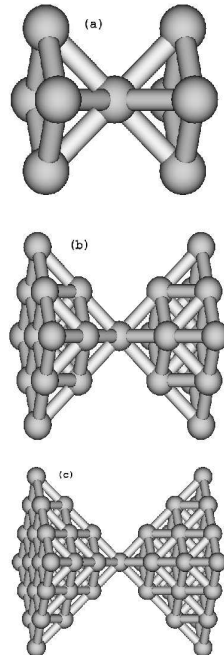


FIG. 2. Atomic structure of the single-atom contact model considered in this work. The number of (001) planes increases by one from (a) to (c) in both electrodes increasing the size of the pyramids and the corresponding atomic detail in the electrode bulk. Interatomic bulk distances have been considered for the whole cluster.

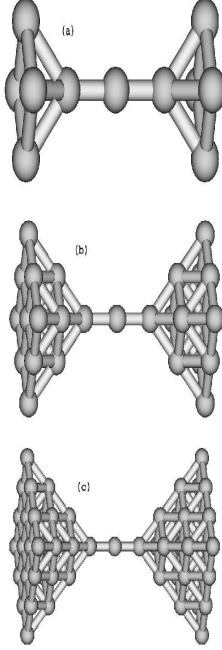


FIG. 3. Atomic structure of the first atom-chain constriction model considered. The number of (001) planes increases by one from (a) to (c) in both electrodes increasing the size of the pyramids and the atomic detail in the electrode bulk. The distance between pyramid apex atoms is  $4.8\text{\AA}$ .

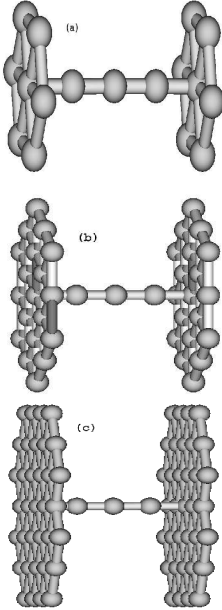


FIG. 4. Atomic structure of the second atom-chain constriction model considered. The number of atoms in the (111) electrode surface increases from (a) to (c) in both electrodes increasing the atomic detail of the surface. The distance between planes is  $9.1\text{\AA}$  and the positions of the atoms in the chain have been optimized.

### 1. Aluminum

Figure 5 (top panel) shows the conductance vs. energy for a single-atom Al contact. We have considered a  $3s3p$  basis set and bulk interatomic distances. Curves (a), (b), and (c) correspond to clusters (a), (b), and (c) in Fig. 2, respectively. In all the clusters the contact between electrodes occurs through a single atom, but the number of (001) planes explicitly included in the DF calculation for each pyramid increases from (a) to (c) (remember that Bethe lattices are always attached to the outer planes as in Fig.1).

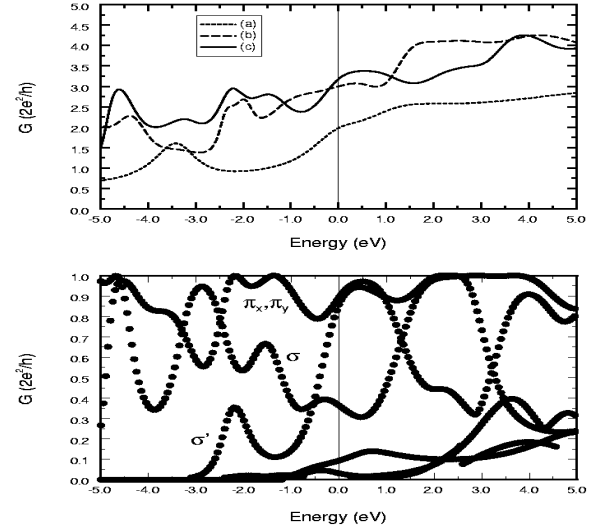


FIG. 5. Top: Conductance versus energy (Fermi energy set to zero) of the single-atom Al contact seen in Fig. 2 for the three cases shown there. Bottom: Individual contribution of the different active conduction channels for (c). The labels indicate the orbital nature of the channels. The primed label is associated with 2nd-nearest-neighbors hoppings.

It is impossible to know the actual atomic structure of the metallic contact in detail unless relaxation calculations are performed, but we do not expect the detailed geometry away from the neck to be important. In fact, as Fig. 5 shows, the conductance does not change significantly from (b) to (c), apart from minor changes in the fine structure. This is a clear indication that, to a good extent, the conductance is determined by the atomic structure in the narrowest region of the neck.

However, from our results we see that, at least, the nine central atoms must be explicitly considered in this example. This is in contrast to the conclusions drawn in Ref. [13] by Cuevas *et al.* using a modified tight-binding model. Furthermore, the value of  $G$  around the Fermi level is  $\approx 3$  which is remarkably different from the value they obtained. This discrepancy is due to a combination of facts. First, the hopping parameters that reproduce bulk properties in tight-binding models are not adequate for atoms with low coordination numbers, being these typically smaller than the *ab-initio* ones. Second, there are non-negligible contributions from next-to-nearest neighbor hoppings in Al. This is clearly seen in the bottom panel of Fig. 5 where the contributions to the total current of the main individual channels for the cluster (c) are depicted. As shown in the figure, a channel associated with 2nd-nearest-neighbors hoppings (labelled  $\sigma'$ ) can give a contribution of almost one conductance quantum  $G_0$  ( $G_0 = 2e^2/h$ ) at the Fermi level. The main contribution at  $\epsilon_F$  comes from two degenerate  $p_x, p_y$ -like channels ( $\pi_x, \pi_y$ ) that account for almost two conductance quanta  $2G_0$ . (The  $z$ -axis has been chosen along the main symmetry axis of the cluster). In addition there are two channels that have  $sp_z$  character ( $\sigma$ ) with non-negligible contributions at the Fermi energy that add approximately  $0.3G_0$  and  $0.1G_0$  to the total conductance, respectively. None of this seems consistent with the tight-binding results for a similar geometry [13].

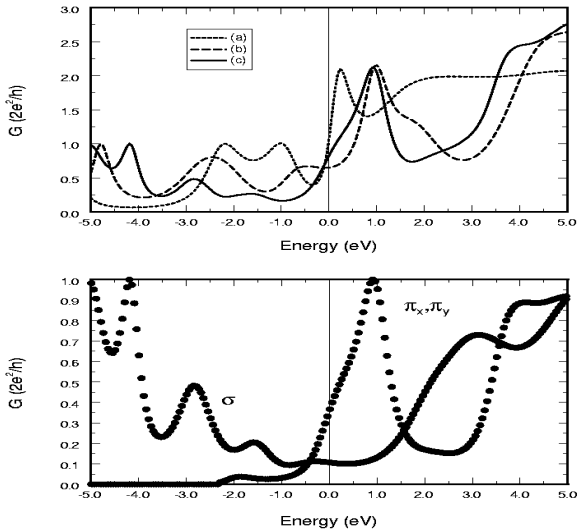


FIG. 6. Same as in Fig. 5, but with three Al atoms forming a linear chain in between the electrodes (see Fig. 3).

The conductance of the three-atom chain shows a different behavior from the one in the previous example and presents the same features for the two electrode models considered (see top panels in Figs. 6 and 7). For the first

electrode model we have chosen a separation of  $4.8\text{\AA}$  between apex atoms of the pyramids. The conductance changes appreciably from (a) to (b) in Fig. 6, but it does not so from (b) to (c). (This dependence is similar to that in the single-atom contact). In the second case we have chosen a separation of  $9.1\text{\AA}$  between planes and we have performed an *ab-initio* relaxation of the chain atom positions (only the surface layer is included in the DF calculation where the number of atoms increases from 7 to 35). Here the conductance does not depend too much on the number of surface atoms [see Figs. 4(a), (b), and (c)]. In all the cases there are oscillations as a function of the energy which, as the bottom panels in Figs. 6 and 7 show, appear mostly in the  $\pi$  channels. This is reminiscent of the behavior of the transmission in a Fabry-Perot interferometer due to scattering at the interfaces. These results are similar to the ones reported in Ref. [21] where a jellium model was used to describe the Al electrodes.

In the three cases considered there is no trace of possible conductance quantization. A general trend that can be observed in our results for the chain is that the onset of the transmission through the  $\pi$  channels occurs close to the Fermi energy [21]. This makes  $G$  strongly dependent on small variations in the positions of the atoms in the chain and on the atomic structure of the electrodes close to the chain. This might explain why the experimental conductance histograms for Al are much more irregular than those for Au (see below) and other metals [4,7]. However, there are many open questions regarding the details of the conductance steps for Al that illustrate the necessity of performing both relaxation and conductance calculations at the same time [46].

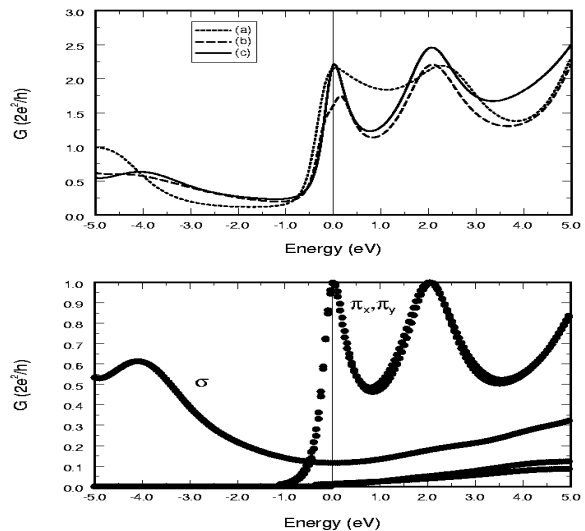


FIG. 7. Same as in Fig. 6, but here the pyramids have been substituted by (111) surface planes. The number of atoms included in the planes are 7(a), 19(b), and 35(c) (see Fig. 4).

## 2. Gold

We have repeated the conductance calculations for the same structures considered above, but now consisting of Au atoms (we have used a here  $5d6s6p$  basis set). In principle, only the electron of the  $6s$  orbital is expected to contribute to the conductance at the Fermi energy which should make the analysis of conductance simpler. As Fig. 8 shows, the conductance around the Fermi energy for the single-atom contact varies little from (a) to (c). We note again that, contrary to the tight-binding predictions [13], the conductance at the Fermi energy surpasses  $G_0$  in all the curves. As concerns the contribution of the individual channels we note that the major contribution (almost a conductance quantum) has  $sp_zd_0$  character ( $\sigma$ ). Two degenerate channels ( $\pi_x, \pi_y$ ) of  $p_xd_1$  and  $p_yd_{-1}$  character (mainly  $d$ ) give around  $0.25G_0$  quanta each. This should be expected since the  $d$  orbitals contribute significantly to the density of states in bulk atoms and the number of near neighbors (eight) of the central atom in this cluster is almost the bulk coordination number of an fcc structure (twelve). Of the two channels that give a significant contribution at rather high energies (above 2.0 eV) one has  $sp_zd_0$  symmetry ( $\sigma$ ) and the other corresponds to 2nd-nearest-neighbors.

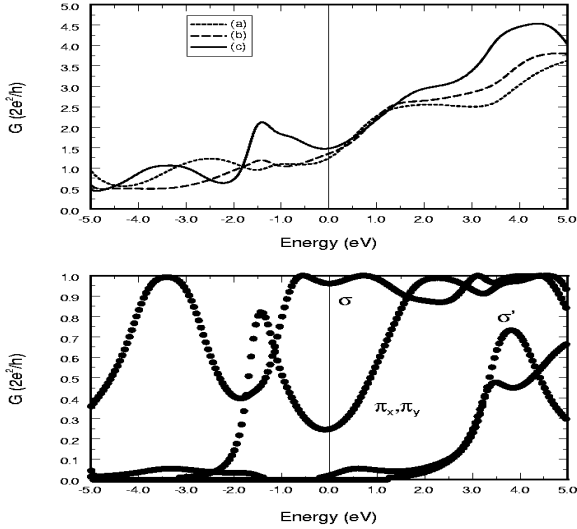


FIG. 8. Top: Conductance versus energy (Fermi energy set to zero) of the single-atom Au contact seen in Fig. 2 for the three cases shown there. Bottom: Individual contribution of the different active conduction channels for (c). The labels indicate the orbital nature of them and  $\sigma'$  indicates 2nd-nearest-neighbors.

It is interesting to compare the single-atom contact results for Al and Au. As remarked above, whereas in the case of Al there was a very important contribution to

the current at the Fermi level coming from 2nd-nearest-neighbors hoppings, in Au this was only appreciable at high energies. This cannot be understood in terms of the respective atomic radii which are very similar (1.43 Å and 1.45 Å for Al and Au, respectively [48]), but rather it is due to the character of the wavefunctions at the Fermi level in each case. Namely, while in Al the density of states at  $E_F$  mainly comes from  $p$  orbitals that are rather extended, in Au the wavefunction at that energy mainly has an  $s$  character and is more localised.

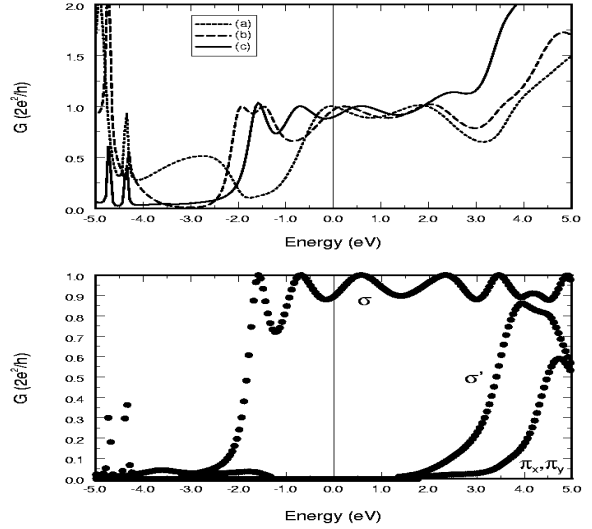


FIG. 9. Same as in Fig. 8, but with three Au atoms forming a linear chain in between the electrodes (see Fig. 3).

On the other hand, the conductance around the Fermi energy for the three-atom Au chain shows clearly an upper limit of  $G_0$  (see top panels in Figs. 9 and 10), and it does not change qualitatively with the cluster size. Nevertheless, the exact value at the Fermi energy is elusive, changing by as much as 20% from cluster to cluster. We have not been able to verify whether the conductance curves for larger clusters converge to a given one, but all the curves present a characteristic behavior: Above the Fermi energy the conductance is fairly constant while below oscillates and vanishes right above the  $d$  channel contribution. The channel decomposition analysis is quite simple: A single  $sp_zd_0$ -like channel ( $\sigma$ ) contributes around the Fermi energy. Nevertheless, it is still difficult to explain from our results the robustness of the quantization observed in the experiments [4,7] which does not deviates from  $G_0$  by more than a small percentage over a large range of stretching force. Large-scale structural studies along with conductance calculations are also desirable here in order to make a precise quantitative comparison with experiments. Recent *ab-initio* works [22,30] for Au nanocontacts have partially

addressed this problem. However, as already pointed out, the electrode model considered there seems to introduce serious difficulties in the interpretation of their conductance results.

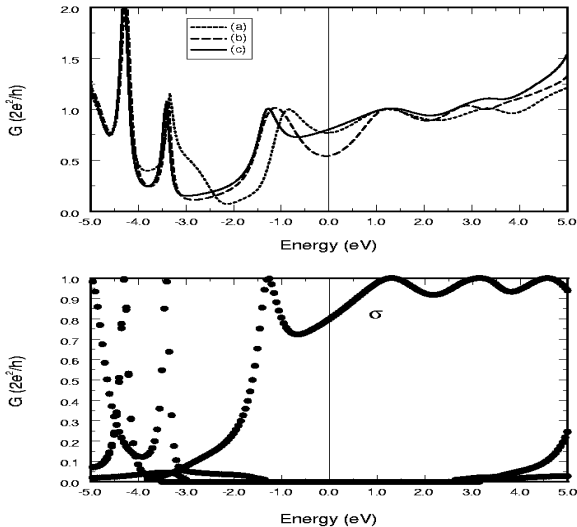


FIG. 10. Same as in Fig. 9, but here the pyramids have been substituted by (111) surface planes. The number of atoms included in the planes are 7(a), 19(b), and 35(c) (see Fig. 4).

## B. Carbon chains

The conductance of C-atom chains attached to Al electrodes has been calculated from first principles in previous works by Lang and Avouris [24,27]. In their calculations semi-infinite jellium models were used to describe the metal electrodes and a pseudopotential for the C cores. The self-consistent density functional procedure they used (see Refs. [24,27] for details) predicted an oscillatory behavior in the conductance at the Fermi level with maxima (minima) in those chains that had an odd (even) number of electrons. This oscillatory behavior differs from that corresponding to a closed shell electronic structure and an  $sp_z$  hybridization of linear C chains. In this situation each C atom added to the chain provides two  $sp$  orbitals that contribute to the  $\sigma$  molecular orbitals (MOs) and two  $p$  orbitals that contribute to the corresponding  $\pi$  MOs. With a closed-shell electronic structure and an *even* number of C atoms there is a partial filled  $\pi$  shell, and the chain could be considered to be intrinsically a conductor. On the other hand, if the chain has an odd number of C atoms, the  $\pi$  and  $\sigma$  shells are completely filled and we would have a semiconductor. Thus, one would expect that chains with an *even* number of C atoms would provide higher conductances than chains

with an *odd* number of C atoms [24]. However, either if we consider an open shell electronic structure for the C chain, or if the edge C atoms are bonded to a metal surface, the MOs can be filled in a different way, which may lead to an *inversion* of the aforementioned trend: that is, chains with an *odd* number of C atoms having a partially filled  $\pi$  shell while chains with an *even* number of C atoms having this shell completely filled. The first scenario, i.e., an open-shell electronic structure, is actually the ground-state for isolated linear C chains, while the second one explains the findings of Lang and Avouris for the conductance of C chains attached to Al electrodes [24,27]. In this second situation the details of the bonding region between the C and metal atoms is of primary importance. This involves knowing the geometry of the contact, the C-metal surface distance, and the electronic structure of the metal under interest. This, however, cannot be easily deduced by using a jellium model to describe the leads.

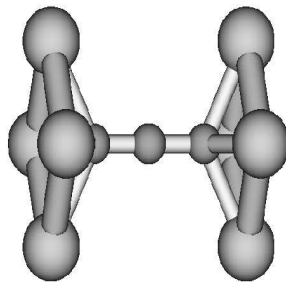


FIG. 11. Atomic structure of a  $C_3$  chain attached to hollow sites in between (001) fcc Al surfaces.

For this reason, we have applied the method described in the previous sections to these kind of systems. More precisely, we have calculated the conductance for C chains starting from 3 C atoms attached to Al and Au (001) fcc electrodes. The distance between C atoms was fixed to that used in Refs. [24,27], i.e., an equal spacing of 2.5 a.u. between C atoms. The description of the electrode surface was reduced to four metal atoms describing a hollow site (see Fig. 11) in the center of which the C chain was attached. The importance of the C-Al surface distance was analyzed by making two sets of calculations for each C chain. In the first set this distance was kept fixed at a reference value of  $2\text{\AA}$ , while in the second one the distance between the C chain and the metal electrode was that providing the minimum energy of the corresponding cluster. The results are commented next.



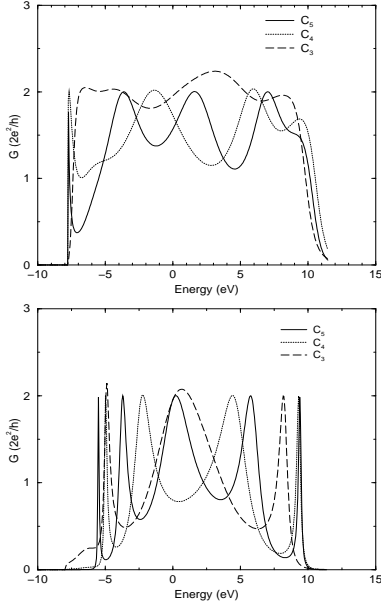


FIG. 12. Top: conductance versus energy (Fermi energy here set to zero) of  $C_n$  linear chains ( $n = 3 - 5$ ) attached to Al at equilibrium C-Al distance ( $1\text{\AA}$ ). Bottom: the same at a distance C-Al of  $2\text{\AA}$ .

### 1. Al electrodes

The discussion about the conductor or semiconductor character of C chains given in the preceding section can be easily extended to the conductance of these chains once they have been contacted to semi-infinite electrodes. Note that the oscillatory character of the conductance at the Fermi level with the number of C atoms  $n$  in the chain found in these systems can be understood as a consequence of the oscillatory nature of the conductance with respect to the energy (reflected in Fig. 12). The oscillations in  $G(E)$  come from *two* degenerate  $\pi$  channels, thus explaining the maximum value of  $2G_0$  (the only exceptions being the  $C_3$  and  $C_4$  chains where additional  $\sigma$  channels appear around the Fermi energy). The number of peaks is given by the number of  $\pi$  orbitals in the chain which, in turn, depends on the number of C atoms present in the chain. The positioning of the Fermi level near the center of these peaks (partially filled  $\pi$  shell) or in between peaks (completely filled  $\pi$  shell) would determine the oscillatory trend with  $n$ . On the other hand, both the exact position of the conductance peaks with respect to the Fermi level and their average size are governed by the distance between the edge of the C chain and the Al electrode.

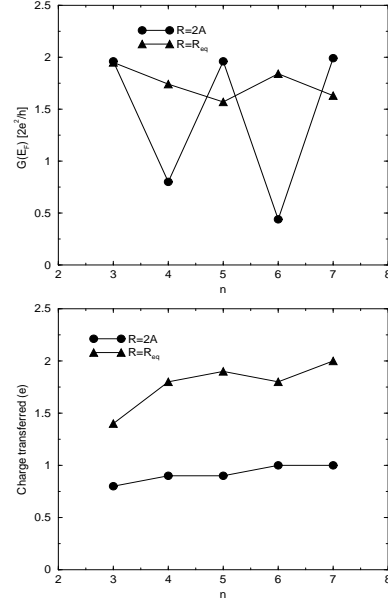


FIG. 13. Top: conductance at the Fermi level of  $C_n$  linear chains ( $n = 3 - 7$ ) attached to Al electrodes. Bottom: charge transferred to the C chain.

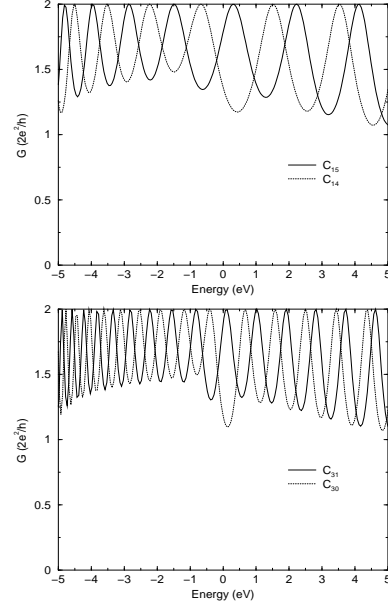


FIG. 14. Top: conductance vs. energy (Fermi energy here set to zero) of  $C_n$  linear chains ( $n = 14, 15$ ) attached to Al electrodes. Bottom: the same for  $n = 30, 31$ .

After inspection of Fig. 12, where we plot the  $G(E)$  for the two sets of calculations mentioned at the beginning of this section, it is evident that at a distance of  $2\text{\AA}$  between the edge C atom and the Al metal surface we end up with the same situation found by Lang and Avouris [24,27], namely, maxima (minima) located at  $n$  odd (even) (see Fig. 13). Nevertheless, at the equilibrium distance, where the C-Al surface distance is smaller ( $1\text{\AA}$ ), and the transferred charge from the metal to the

C chain is larger, the situation has changed and now the maxima are located on chains with an even number of C atoms (the only exception being again the  $C_3$  chain) as Fig. 13 shows. However, one would expect that the influence of the bonding region, a local effect, would become less important as the size of the C chain increases. This is what is actually found in the conductance of larger number of atoms, such as those presented in Fig. 14, where we plot  $G(E)$  for  $n=14,15$  and for  $n=30,31$  and a distance C-Al surface of  $1\text{\AA}$ . In both cases the chains with  $n$  odd give larger values for  $G(\epsilon_F)$  than those with  $n$  even. The same behavior is found for the same chains attached to Al electrodes at a distance of  $2\text{\AA}$ , but has not been included in the figures for simplicity. It is worth noting that, strictly speaking at zero temperature, the peaks in  $G(E)$  and, thus, the oscillations in  $G(\epsilon_F)$  are expected to survive in the thermodynamic limit  $n \rightarrow \infty$ . This effect will disappear when the temperature becomes of the same magnitude as the peaks width, where  $G(\epsilon_F)$  will be the average value for the odd- and even- $n$  chains.

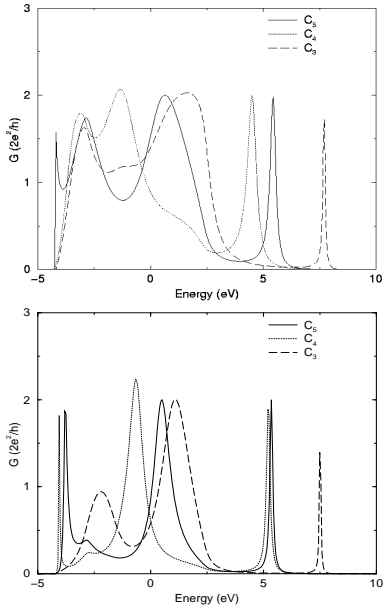


FIG. 15. Top: conductance versus energy (Fermi energy here set to zero) of  $C_n$  linear chains ( $n = 3 - 5$ ) attached to Au at equilibrium C-Au distance ( $1.5\text{\AA}$ ). Bottom: the same at a distance C-Au of  $2\text{\AA}$ .

## 2. Au electrodes

Another key point in the conductance of nanocontacts is the nature of the metal used in the electrodes which has been thoroughly discussed in previous sections. This is specially the case when the chemical bond between the molecule and the metal contact changes markedly as reflected in Fig. 15 as compared to Fig. 12. There we show  $G(E)$  for the same systems previously analyzed for Al but with Au instead. When we move from Al to Au

the bonding between the C chain and the metal surface weakens. This reflects in a sharpening of the conductance peaks and in the amount of charge transferred from the metal to the C chain (compare Figs. 16 and 13). The equilibrium distance between the edge C atom and the Au surface is also typically larger in this case:  $1.5\text{\AA}$  for all the chains. As for Al, there also appear two  $\pi$  channels, except for the  $C_3$  and  $C_4$  chains. However, the narrowing of the conductance peaks makes critical the alignment of the Fermi level. With respect to the oscillations of  $G(\epsilon_F)$ , we observe the same tendency irrespective of the C-Au distance, that is: maxima located at  $n$  odd. This is also a consequence of the weaker bond between Au and C and the lesser amount of charge transferred from the former to the latter.

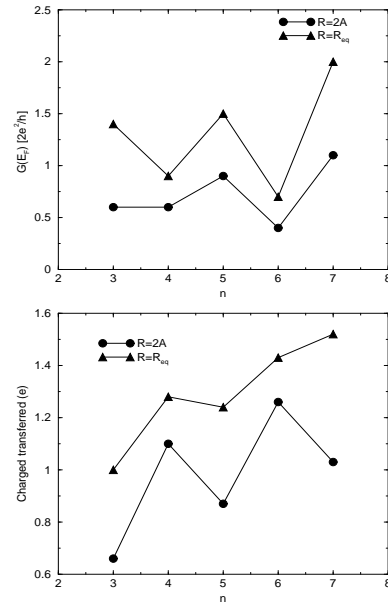


FIG. 16. Top: conductance at the Fermi level of  $C_n$  linear chains ( $n = 3 - 7$ ) attached to Au electrodes. Bottom: charge transferred to the C chain.

## IV. CONCLUDING REMARKS

In summary, we have developed a methodology to self-consistently calculate *ab-initio* transport properties in atomic-scale systems based upon the Gaussian98 code. This opens the doors to the use of the most standard quantum chemistry tool to the study of transport through molecules, an interdisciplinary subject of increasing interest. We have chosen to study two systems that illustrate the capabilities of our approach: metallic constrictions of simple and noble metals and C chains with a reactive electrode (Al) and an “inert” (Au) electrode. In the first case, we have shown that assuming local charge neutrality, as commonly done in semi-empirical methods, may lead to qualitatively incorrect results. On the other hand, the system metal-C

chain-metal illustrated how the chemistry of the contact may determine electrical transport and, therefore, the incorrectness of ascribing one or another behavior to a given molecule leaving apart the specific electrode/molecule chemistry. One should speak, instead, of electrical transport characteristics of the whole system, electrode-molecule-electrode.

## ACKNOWLEDGMENTS

Part of this work was supported by the Spanish CICYT under Grants Nos. 1FD97-1358 and PB96-0085, and by the Generalitat Valenciana under Grants No. GV00-151-01 and GV00-095-2. Discussions with L. Pastor-Abia, J. M. Pérez-Jordá, J. C. Sancho, N. Agraït, P. Serena, A. Hasmy, D. Sánchez-Portal, C. Untiedt, F. Guinea, and J. J. Sáenz are acknowledged. We are also grateful to D. A. Papaconstantopoulos for useful correspondence concerning the tight-binding parameters used in band structure calculations.

## V. APPENDIX

In this appendix we discuss how selfenergies for Bethe Lattices (BL) with no symmetry can be calculated. Symmetry can be broken due to either the spatial atomic arrangement or the orbitals on the atoms that occupy each lattice site, or both. When no symmetry exists the self-energy in an arbitrary direction cannot be obtained by rotating that for a given direction as done in Ref. [34]. Instead, the following procedure has to be followed. The method is valid for any basis set or lattice. Let  $\tau_i$  be the  $N$  nearest-neighbor directions of the lattice we are interested in and  $\hat{V}_{\tau_i}$  the interatomic interaction matrix in these directions. The selfenergies associated to each direction have to be obtained from the following set of  $2N$  coupled selfconsistent equations,

$$\hat{\Sigma}_{\tau_i} = \hat{V}_{\tau_i} \left[ E\hat{1} - \hat{E}_0 - (\hat{\Sigma}_{\bar{T}} - \hat{\Sigma}_{\bar{\tau}_i}) \right]^{-1} \hat{V}_{\tau_i}^\dagger \quad (6a)$$

$$\hat{\Sigma}_{\bar{\tau}_i} = \hat{V}_{\bar{\tau}_i} \left[ E\hat{1} - \hat{E}_0 - (\hat{\Sigma}_T - \hat{\Sigma}_{\tau_i}) \right]^{-1} \hat{V}_{\bar{\tau}_i}^\dagger, \quad (6b)$$

where  $i = 1, \dots, N$  and  $\bar{\tau}_i = -\tau_i$ .  $E\hat{1}$  is the energy times the identity matrix,  $\hat{E}_0$  is a diagonal matrix containing the orbital levels,  $\hat{V}_{\tau_i}$  is the interatomic interaction in the  $\tau_i$  direction, and  $\hat{\Sigma}_T$  and  $\hat{\Sigma}_{\bar{T}}$  are the sums of the selfenergy matrices entering through all the Cayley tree branches attached to an atom and their inverses, respectively, *i.e.*,

$$\hat{\Sigma}_T = \sum_{i=1}^N \hat{\Sigma}_{\tau_i} \quad (7a)$$

$$\hat{\Sigma}_{\bar{T}} = \sum_{i=1}^N \hat{\Sigma}_{\bar{\tau}_i}. \quad (7b)$$

This set of  $2N$  matricial equations has to be solved iteratively. It is straightforward to check that, in cases of full symmetry, it reduces to the single equation discussed in [34].

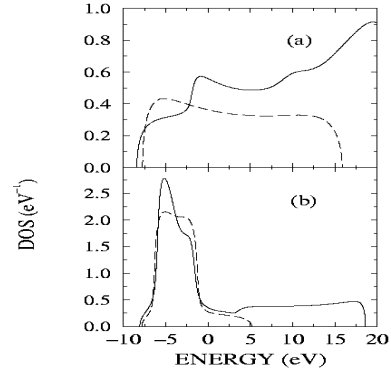


FIG. 17. Density of states for the Bethe lattices of Al (a) and Au (b) obtained with the parameters of Table I. Continuous lines correspond to results obtained with a *spd* basis while broken lines to those obtained with either a *sp* (Al) or a *sd* (Au) basis. The Fermi level was set at zero energy.

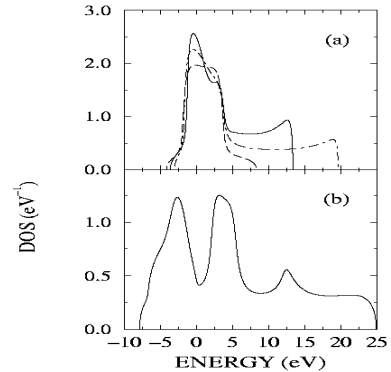


FIG. 18. Density of states for the Bethe lattices of Ti (a) and W (b) obtained with the parameters of Table II. Continuous lines correspond to results obtained with a *spd* basis and the hcp and bcc lattices for Ti and W, respectively. In the case of Ti two further curves are given which correspond to the fcc lattice with a *spd* basis (broken line) or a *sd* basis (chain line). The Fermi level was set at zero energy.

The tight-binding parameters, which include only nearest-neighbors interactions, used in these calculations are given in Table I. The Table reports data not only for the metals taken as electrodes in the present work (Al and Au) but also for two additional metals (Ti and W) commonly used in experiments and/or calculations. All were obtained through fittings to the electronic bulk band structures calculated by including second or even third nearest-neighbors interactions [49]. In the case of hexagonal-close-packed Ti we took as nearest-neighbors

six out of plane and six in-plane neighbors, as actual interatomic distances differ in less than a 2% [50]. The densities of states on bulk atoms are shown in Fig. (17) and (18). Although some of the features of the actual DOS are not reproduced (as it commonly occurs in the Bethe lattice approximation) the overall results are satisfactory. The major discrepancy is noted for Ti since in this metal the Fermi level in the crystalline case lies in a valley of the DOS [49]. In the calculations reported in this work the *sp* basis was used for Al. We have described the electronic structure of Au by means of the *spd* basis (see Fig. 17 and Table I). In the case of Au and Ti, the reduced *sd* basis gives an excessively narrow conduction band. Finally, we note that in the case of Ti there are no major differences between the DOS for the fcc and hcp lattices.

- 
- [1] For recent reviews on this issue see C. Joachim, J. K. Gimzewski, and A. Aviram, *Nature* **408**, 541 (2000); A. Nitzan, *Annu. Rev. Phys. Chem.* **52** 681 (2001).
- [2] D. Porath *et al.*, *Phys. Rev. B* **56**, 9829 (1997); J. G. Hou *et al.*, *Phys. Rev. Lett.* **83**, 3001 (1999); J. I. Pascual *et al.*, *Chem. Phys. Lett.* **321**, 78 (2000).
- [3] J. I. Pascual *et al.*, *Phys. Rev. Lett.* **85**, 2653 (2000); J. G. Hou *et al.*, *Phys. Rev. Lett.* **85**, 2654 (2000).
- [4] N. Agraït, J. C. Rodrigo, and S. Vieira, *Phys. Rev. B* **47**, 12345 (1993); J. I. Pascual *et al.*, *Phys. Rev. Lett.* **71**, 1852 (1993); N. Agraït, G. Rubio, and S. Vieira, *Phys. Rev. Lett.* **74**, 3995 (1995); G. Rubio, N. Agraït, and S. Vieira, *Phys. Rev. Lett.* **76**, 2302 (1996); C. Untiedt, G. Rubio, S. Vieira, and N. Agraït, *Phys. Rev. B* **56**, 2154 (1997); J. I. Pascual *et al.*, *Science* **267**, 1793 (1995); H. Ohnishi, Y. Kondo, and K. Takayanagi, *Nature (London)* **395**, 780 (1998); J. L. Costa-Krämer *et al.*, *Phys. Rev. B* **55**, 5416 (1997); J. L. Costa-Krämer, N. García, and H. Olin, *Phys. Rev. Lett.* **78**, 4990 (1997); G. Rubio-Bollinger *et al.*, *arXiv:cond-mat/0105277* (unpublished); N. Agraït *et al.*, *arXiv:cond-mat/0110601* (unpublished).
- [5] For a nice review on nanotubes see C. Dekker, *Phys. Today* **52**, No. 5, 22 (1999).
- [6] P. J. de Pablo *et al.*, *Phys. Rev. Lett.* **85**, 4992 (2000).
- [7] C. J. Muller, J. M. vanRuitenbeek, and L. J. de Jong, *Phys. Rev. Lett.* **69**, 140 (1992); *ibid.* *Physica C* **191**, 485 (1992); J. M. Krans *et al.*, *Phys. Rev. B* **48**, 14721 (1993); J. M. Krans *et al.*, *Nature (London)* **375** 767 (1995); A. I. Yanson and J. M. vanRuitenbeek, *Phys. Rev. Lett.* **79**, 2157 (1997); E. Scheer *et al.*, *Nature* **394**, 154 (1998).
- [8] M. A. Reed *et al.*, *Science* **278**, 252 (1997).
- [9] C. Kergueris *et al.*, *Phys. Rev. B* **59**, 12505 (1999); H. Park *et al.*, *Nature* **407**, 57 (2000).
- [10] For a review on the issue see S. Datta, *Electronic transport in mesoscopic systems*, ed. by H. Ahmed, M. Pepper, and A. Broers (Cambridge University Press, Cambridge, 1995).
- [11] An extension to non-equilibrium transport including many-body effects has also been developed by means of Keldysh techniques. See, e.g., Y. Meir and N. S. Wingreen, *Phys. Rev. Lett.* **68**, 2512 (1992); S. Hershfield, J. H. Davies, and J. W. Wilkins, *Phys. Rev. Lett.* **67**, 3720 (1991). Landauer's description emerges in this case as the limiting case for zero bias and zero temperature.
- [12] C. Joachim *et al.*, *Phys. Rev. Lett.* **74**, 2102 (1995); C. Joachim, J. K. Gimzewski, and H. Tang, *Phys. Rev. B* **58**, 16407 (1998); V. Mujica, M. Kemp, and M. Ratner, *J. Chem. Phys.* **101**, 6849 (1994); S. Datta *et al.*, *Phys. Rev. Lett.* **79**, 2530 (1997); Y. Xue *et al.*, *Phys. Rev. B* **59**, 7852 (1999); S. N. Yaliraki and M. A. Ratner, *J. Chem. Phys.* **109**, 5036 (1998); E. G. Emberly and G. Kirczenow, *Phys. Rev. B* **58**, 10911 (1998).
- [13] J. C. Cuevas *et al.*, *Phys. Rev. Lett.* **80**, 1066 (1998); J. C. Cuevas *et al.*, *Phys. Rev. Lett.* **81**, 2990 (1998).
- [14] M. Brandbyge, N. Kobayashi, and M. Tsukada, *Phys. Rev. B* **60**, 17064 (1999); K. Hansen *et al.*, *Appl. Phys. Lett.* **77**, 708 (2000).
- [15] M. Paulsson and S. Stafström, *Phys. Rev. B* **64**, 035416 (2001).
- [16] *Gaussian 98*, Gaussian Inc., Pittsburgh, PA, 1998.
- [17] P. Ordejón, E. Artacho, and J. M. Soler, *Phys. Rev. B* **53** R10441 (1996); D. Sánchez-Portal, P. Ordejón, E. Artacho, and J. M. Soler, *Int. Jour. of Quant. Chem.* **65**, 453 (1999).
- [18] N. D. Lang, *Phys. Rev. B*, **52**, 5335 (1995).
- [19] K. Hirose and M. Tsukada, *Phys. Rev. B* **51**, 5278 (1995).
- [20] J. Taylor, H. Guo and J. Wang, *Phys. Rev. B* **63**, 245407 (2001).
- [21] N. Kobayashi, M. Aono, and M. Tsukada, *Phys. Rev. B* **64**, 121402 (2001); N. Kobayashi, M. Brandbyge, and M. Tsukada, *Phys. Rev. B* **62**, 8430 (2000).
- [22] M. Brandbyge, J. Taylor, K. Stokbro, J. L. Mozos, and P. Ordejón, *arXiv:cond-mat/0110650* (unpublished).
- [23] S. N. Yaliraki *et al.*, *J. Chem. Phys.* **111**, 6997 (1999); Y. Xue, S. Datta, and M. A. Ratner, *arXiv:cond-mat/0112136* (unpublished).
- [24] N. D. Lang and Ph. Avouris, *Phys. Rev. Lett.* **81**, 3515 (1998).
- [25] G. Taraschi *et al.*, *Phys. Rev. B* **58**, 13138 (1998).
- [26] C. C. Wan, J.-L. Mozos, G. Taraschi, J. Wang, and H. Guo, *Appl. Phys. Lett.* **71**, 419 (1997).
- [27] N. D. Lang and Ph. Avouris, *Phys. Rev. Lett.* **84**, 358 (2000).
- [28] M. Di Ventra, S.-G. Kim, S. T. Pantelides, and N. D. Lang, *Phys. Rev. Lett.* **86**, 288 (2001).
- [29] J. Taylor, H. Guo, and J. Wang, *Phys. Rev. B* **63**, 121104 (2001).
- [30] H. Mehrez *et al.*, *arXiv:physics/0106027* (unpublished).
- [31] F. Guinea, C. Tejedor, F. Flores and E. Louis, *Phys. Rev. B* **28**, 4397 (1983).
- [32] M. P. López Sancho, J. M. López Sancho and J. Rubio, *J. Phys. F: Met. Phys.* **14**, 1205 (1984).
- [33] J. J. Palacios, A. J. Pérez-Jiménez, E. Louis and J. A. Vergés, *Phys. Rev. B* **64**, 115411 (2001).
- [34] L. Martín-Moreno and J. A. Vergés, *Phys. Rev. B* **42**, 7193 (1990); E. Louis and F. Yndurain, *Phys. Rev. B*

- 16**, 1542 (1977).
- [35] J. D. Joannopoulos and F. Yndurain, Phys. Rev. B **10**, 5164 (1974).
  - [36] J. Heurich, J. C. Cuevas, W. Wenzel, and G. Schön, arXiv:cond-mat/0110147 (unpublished).
  - [37] J. M. Pérez-Jordá, E. San-Fabián, and F. Moscardó, Comput. Phys. Commun. **70**, 271 (1992).
  - [38] A. D. Becke, J. Chem. Phys. **98**, 5648 (1993).
  - [39] L. F. Pacios and P. A. Christiansen, J. Chem. Phys. **82**, 2664 (1985).
  - [40] M. M. Hurley, L. F. Pacios, P. A. Christiansen, R. B. Ross and W. C. Ermler, J. Chem. Phys. **84**, 6840 (1986).
  - [41] R. B. Ross, J. M. Powers, T. Atashroo, W. C. Ermler, L. A. LaJohn, and P. A. Christiansen, J. Chem. Phys. **93**, 6654 (1990).
  - [42] P. Schwerdtfeger, J. R. Brown, J. K. Laerdhal, and H. Stoll, J. Chem. Phys. **113**, 7110 (2000).
  - [43] A. Hasmy, E. Medina, and P. A. Serena, Phys. Rev. Lett. **86**, 5574 (2001).
  - [44] D. Sánchez-Portal *et al.*, Phys. Rev. Lett. **83**, 3884 (1999).
  - [45] A. Nakamura, M. Brandbyge, L. B. Hansen, and K. W. Jacobsen, Phys. Rev. Lett. **82**, 1538 (1999).
  - [46] A. Hasmy, J. J. Palacios, A. Pérez-Jiménez, and P. Serena (unpublished).
  - [47] R. Fasel *et al.*, Phys. Rev. Lett. **76**, 4733 (1996).
  - [48] S. Fraga, J. Karowski and K.M.S. Saxena, *Handbook of atomic data* (Elsevier, Amsterdam, 1976).
  - [49] D.A. Papaconstantopoulos, *Handbook of the band structure of elemental solids* (Plenum Press, New York and London, 1986).
  - [50] N.W. Ashcroft and N.D. Mermin, *Solid State Physics* (Saunders College Publishing, New York, 1976).

TABLE I. Tight-binding parameters (in Rydbergs) used in the calculation of the density of states and selfenergies of the Bethe lattices for the metals commonly taken as electrodes, namely, aluminium, gold, titanium and tungsten (the last two not considered in the present work). Orbital on-site energies are represented by  $e_i$  while nearest-neighbor interactions are denoted by  $v_i$ . The electronic configuration taken in each case are: Al-a ( $3s^2 3p^1$ ), Al-b ( $3s^2 3p^1 3d^0$ ), Au-a ( $5d^{10} 6s^1$ ), Au-b ( $5d^{10} 6s^1 6p^0$ ), Ti-a and Ti-c ( $3d^2 4s^2 4p^0$ ), Ti-b ( $3d^2 4s^2$ ) and W ( $5d^4 6s^2 6p^0$ ). Actual lattices are: aluminium and gold, face-centered-cubic, titanium, (a) hexagonal-close-packed and (b) and (c) face-centered-cubic, and wolframium, body-centered-cubic. The parameters were obtained by fitting the bulk electronic band structures given in [49]. The Fermi level  $\epsilon_F$  corresponding to these parameters is also given.

Parameter	Al-a	Al-b	Au-a	Au-b	Ti-a	Ti-b	Ti-c	W
$e_s$	0.35512	0.50658	0.41996	0.51034	0.88100	0.73609	1.07296	0.61616
$e_p$	0.88653	1.05686	-	1.28039	1.15042	-	1.38106	1.46304
$e_{d_{xy}}$	-	1.73644	0.22963	0.27529	0.69449	0.65165	0.69143	1.12072
$e_{d_{xz}}$	-	1.73644	0.22963	0.27529	0.68617	0.65165	0.69143	1.12072
$e_{d_{yz}}$	-	1.73644	0.22963	0.27529	0.68617	0.65165	0.69143	1.12072
$e_{d_{x^2-y^2}}$	-	1.64457	0.22930	0.25542	0.69449	0.63735	0.67293	1.04350
$e_{d_{3z^2-r^2}}$	-	1.64457	0.22930	0.25542	0.69828	0.63735	0.67293	1.04350
$v_{ss\sigma}$	-0.04852	-0.06225	-0.06682	-0.06931	-0.06809	-0.06353	-0.07960	-0.07315
$v_{sp\sigma}$	-0.08296	-0.08914	-	0.08543	0.07676	-	0.11204	-0.00419
$v_{sd\sigma}$	-	0.08741	-0.03868	-0.05282	0.04883	-0.04223	-0.04567	-0.07323
$v_{pp\sigma}$	0.19317	0.16491	-	0.17166	0.09883	-	0.17587	0.37460
$v_{pp\pi}$	0.06339	-0.00999	-	-0.01084	-0.01646	-	-0.00386	0.08730
$v_{pd\sigma}$	-	-0.17352	-	-0.09305	0.06692	-	-0.05580	-0.23996
$v_{pd\pi}$	-	0.04472	-	0.01008	-0.02718	-	0.03158	-0.06160
$v_{dd\sigma}$	-	-0.16416	-0.04391	-0.04872	-0.05211	-0.04337	-0.04794	-0.18762
$v_{dd\pi}$	-	0.07776	0.03367	0.02494	0.02862	0.03907	0.03542	-0.06543
$v_{dd\delta}$	-	-0.01279	-0.00874	-0.00462	-0.00603	-0.00462	-0.00985	0.06917
$\epsilon_F$	6.98	8.24	6.84	7.16	7.83	8.02	7.89	10.45